eLIFE elifesciences.org

RESEARCH ARTICLE

Figures and figure supplements

The horizontally-acquired response regulator SsrB drives a *Salmonella* lifestyle switch by relieving biofilm silencing

Stuti K Desai *et al*

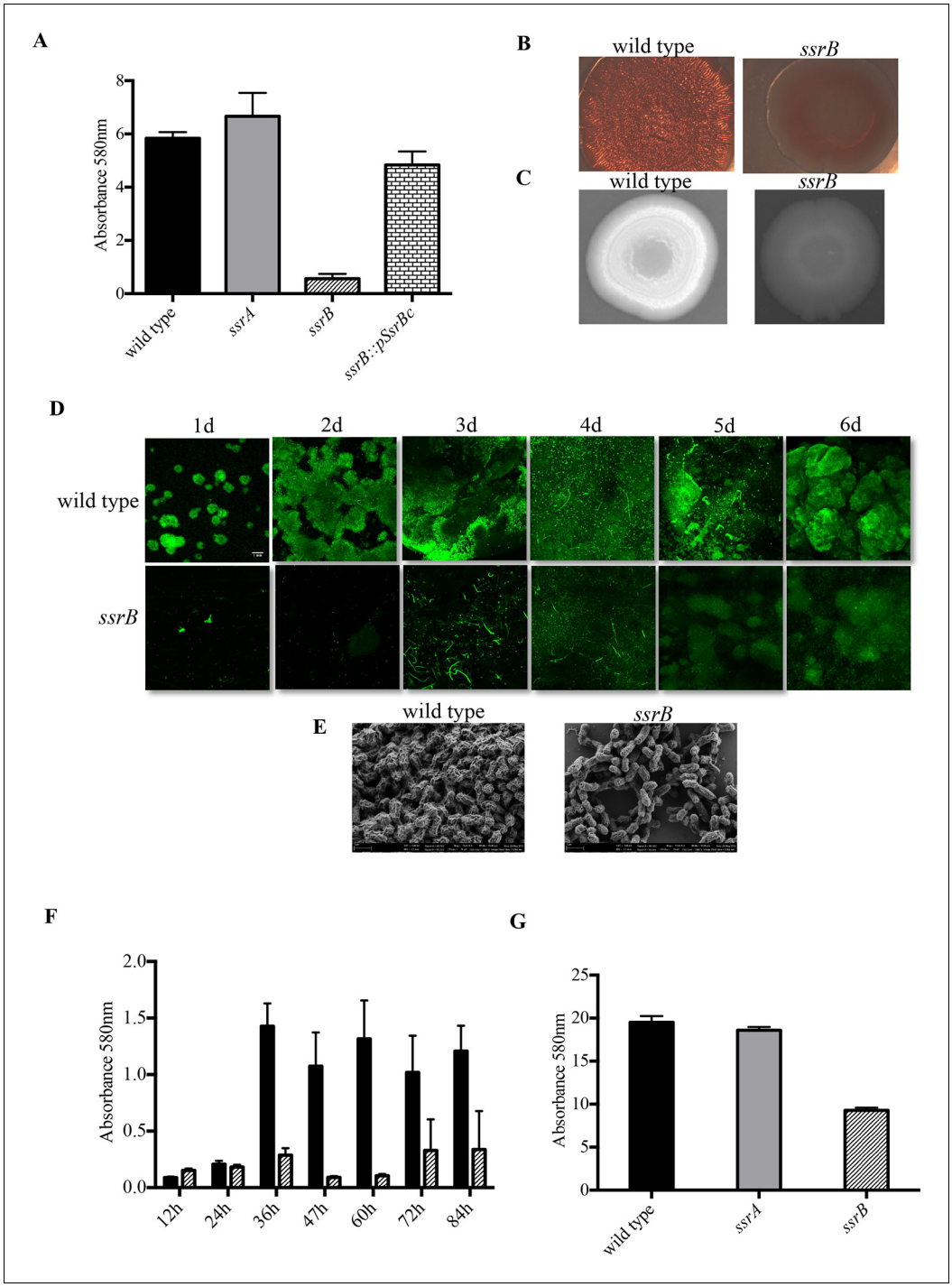

Figure 1. Loss of *ssrB* but not *ssrA* decreases *Salmonella* Typhimuirum biofilms. (**A**) The defect in formation of biofilms in the *ssrB* null was complemented by the overexpression of SsrBc from plasmid pKF104 *in trans* as measured by crystal violet staining. (**B**) The typical rdar morphotype of the wild type strain was lost in the *ssrB* strain as shown on congo red plates. (**C**) A two day old macrocolony of the *ssrB* strain is not fluorescent under UV light with Fluorescent Brightener 28. (**D**) The wild type strain forms thick solid-surface biofilms, while the *ssrB* strain remains poor for biofilms as monitored for six days by SYTO-9 staining of flow cell biofilms; scale bar = 1 mm. (**E**) SEM images showing extensive mesh-like network of wild type biofilms and sparse extracellular matrix of the *ssrB* biofilms; scale bar = 1 µm. (**F**) The amount of biofilms formed by the wild type strain (solid black bars) increases after 24 hr but the *ssrB* null (hatched black bars) remains defective up to 84 hr. n = 2, Mean ± SD, $p < 0.0001$ between wild type and *ssrB* strains from 36 hr till 84 hr. (**G**) The amount of cholesterol-attached biofilms formed by

Figure 1 continued on next page

Figure 1 continued

the *ssrB* strain were significantly less than that produced by the wild type. n = 3, Mean ± SD, $p < 0.0001$. Source data file: ***Figure 1—source data 1***.

DOI: http://dx.doi.org/10.7554/eLife.10747.003

The following source data is available for figure 1:

Source data 1. Source data for crystal violet staining in ***Figure 1A,F and G***.

DOI: http://dx.doi.org/10.7554/eLife.10747.004

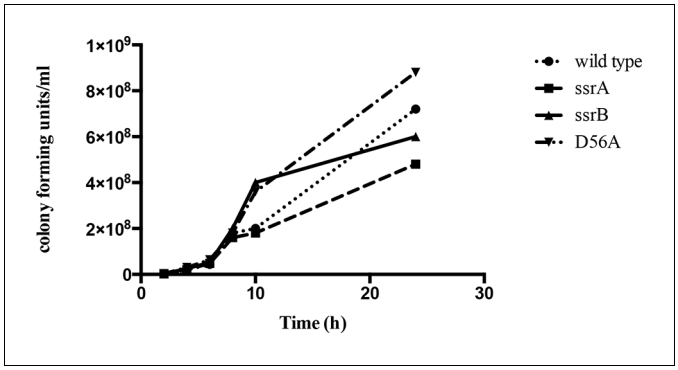

Figure 1—figure supplement 1. The *ssrB* mutant is not defective in growth compared to the wild type strain. Number of colonies formed by the wild type, *ssrA, ssrB* and D56A strains were the same order of magnitude across all the time points tested. Source data file: ***Figure 1—figure supplement 1—source data 1***.
DOI: http://dx.doi.org/10.7554/eLife.10747.005
The following source data is available for figure 1:

Figure supplement 1—Source data 1. Growth curves of wild type, *ssrA, ssrB* and D56A strains.
DOI: http://dx.doi.org/10.7554/eLife.10747.006

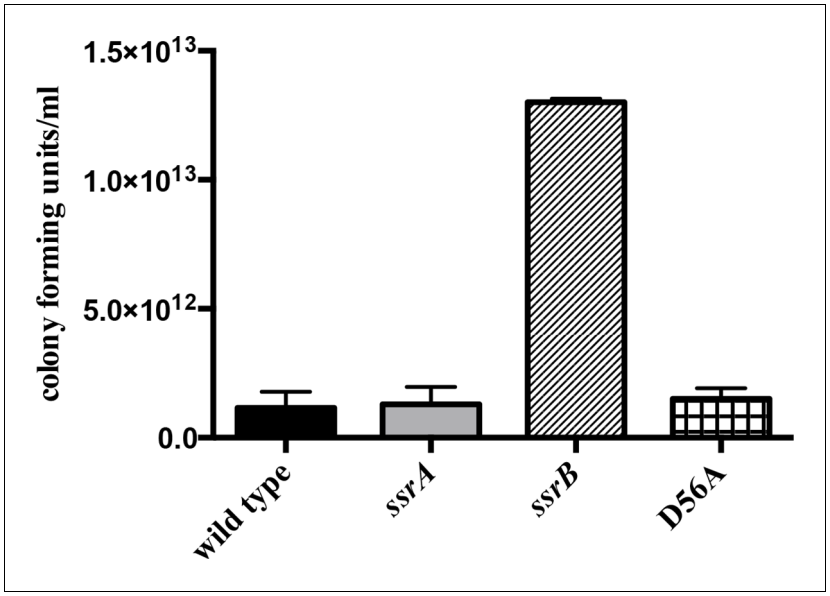

Figure 1—figure supplement 2. The planktonic sub-population of the *ssrB* strain was higher by two orders of magnitude compared to the wild type, *ssrA* and *D56A* strains at 2 days. n = 2, Mean ± SD, $p < 0.05$. Source data file: ***Figure 1—figure supplement 2—source data 1***.

DOI: http://dx.doi.org/10.7554/eLife.10747.007

The following source data is available for figure 1:

Figure supplement 2—Source data 1. Number of cells in the planktonic sub-population of each strain.

DOI: http://dx.doi.org/10.7554/eLife.10747.008

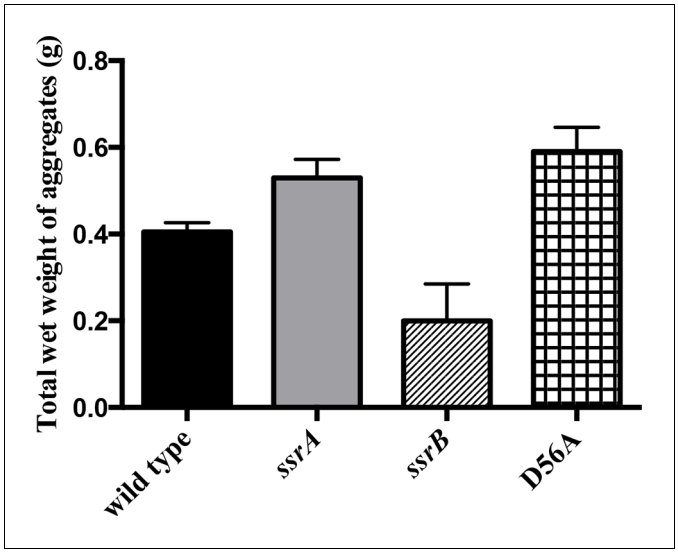

Figure 1—figure supplement 3. Total wet weight of the adherent sub-population was decreased by at least 50% in the *ssrB* strain compared to the wild type, *ssrA* and D56A strains at 2 days. n = 2, Mean ± SD, $p < 0.05$ for the *ssrB* strain versus *ssrA*/D56A strains and $p = 0.08$ for the *ssrB* strain versus wild type. Source data file: ***Figure 1—figure supplement 3—source data 1***.

DOI: http://dx.doi.org/10.7554/eLife.10747.009

The following source data is available for figure 1:

Figure supplement 3—Source data 1. Total wet weight of the adherent sub-population of each strain.

DOI: http://dx.doi.org/10.7554/eLife.10747.010

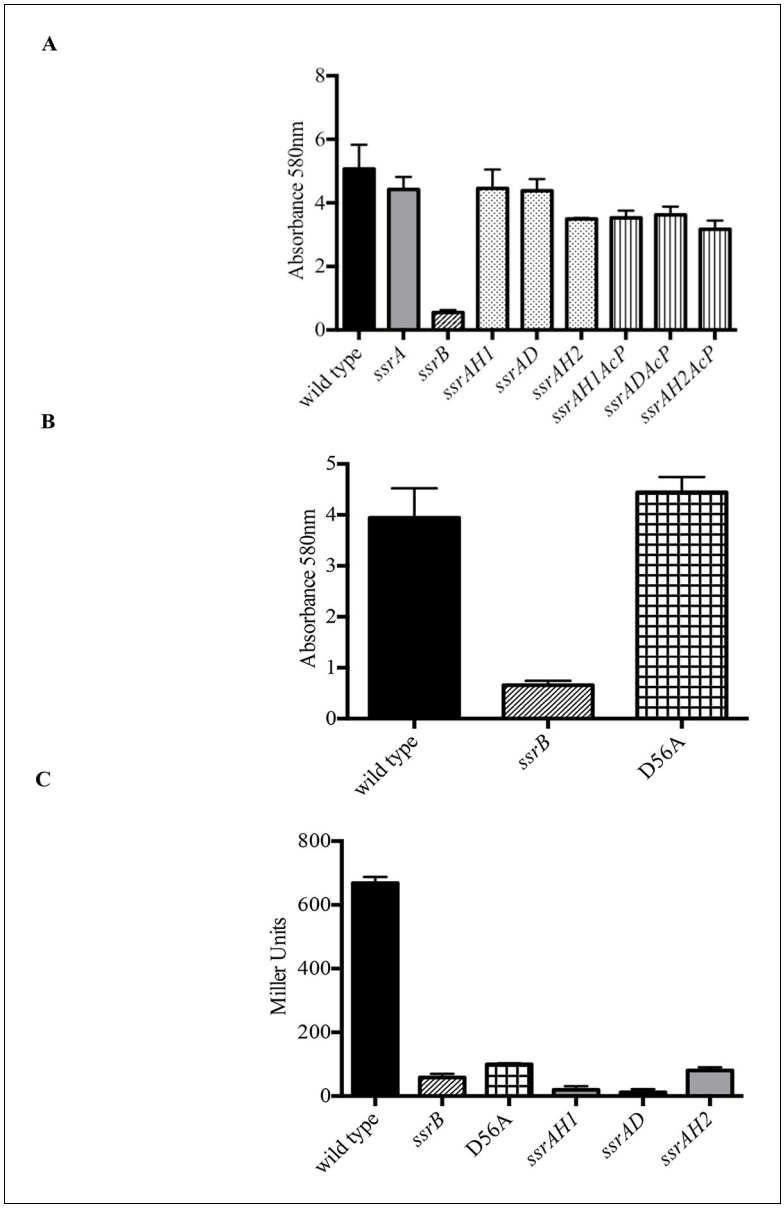

Figure 2. Phosphorylation of SsrB is not required for biofilm formation. Amount of biofilms formed as measured by crystal violet staining for (**A**) Strains *ssrAH1, ssrAD, ssrAH2, ssrAH1AcP, ssrADAcP, ssrAH2AcP* and (**B**) D56A SsrB shows similar levels to that of the wild type, and higher than the *ssrB* mutant. Source data file: ***Figure 2—source data 1***. (**C**) Beta-galactosidase activity of a *sifA-lacZ* chromosomal fusion was significantly lower in the *ssrB* null and the D56A SsrB mutant compared to the wild type. n = 3, Mean ± SD, $p < 0.0001$. Source data file: ***Figure 2—source data 2***.

DOI: http://dx.doi.org/10.7554/eLife.10747.011

The following source data is available for figure 2:

Source data 1. Source data for crystal violet staining in ***Figure 2A and B***.

DOI: http://dx.doi.org/10.7554/eLife.10747.012

Source data 2. Source data for the measurement of beta-galactosidase activity in ***Figure 2C***.

DOI: http://dx.doi.org/10.7554/eLife.10747.013

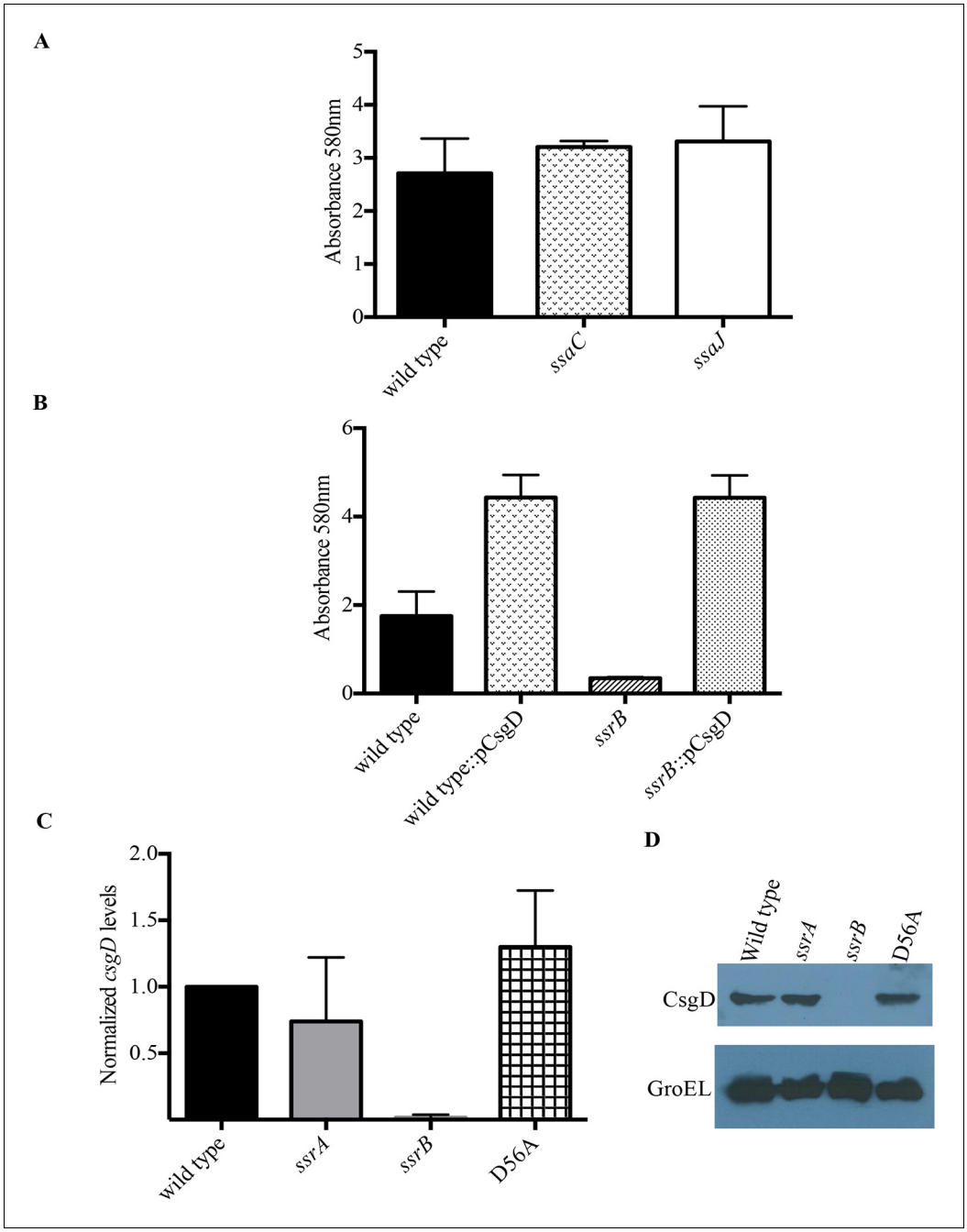

Figure 3. SsrB regulates biofilms by a CsgD-dependent mechanism. (**A**) The SPI-2 needle, *ssaC* and *ssaJ* mutant strains were not affected in biofilm formation. (**B**) Over-expression of *csgD* from a plasmid (pBR328::csgD) *in trans* rescued biofilm formation in the *ssrB* mutant, as measured by crystal violet staining, n = 3. Source data file: ***Figure 3—source data 1***. An estimate of *csgD* expression by (**C**) Real-time qRT-PCR showed a significant decrease in *csgD* transcription in the *ssrB* null, but not in the D56A SsrB and *ssrA* mutants. *rrsA* transcript levels were used as control; n = 2, Mean ± SD, $p < 0.0001$. Source data file: ***Figure 3—source data 2*** and (**D**) Immunoblot analysis showing the absence of CsgD in the *ssrB* null strain in two day old biofilms, using GroEL as a loading control.

DOI: http://dx.doi.org/10.7554/eLife.10747.014

The following source data is available for figure 3:

Source data 1. Source data for crystal violet staining in ***Figure 3A and B***.

DOI: http://dx.doi.org/10.7554/eLife.10747.015

Source data 2. Source data for Real-time qRT-PCR in ***Figure 3C***.

Figure 3 continued on next page

Figure 3 continued

DOI: http://dx.doi.org/10.7554/eLife.10747.016

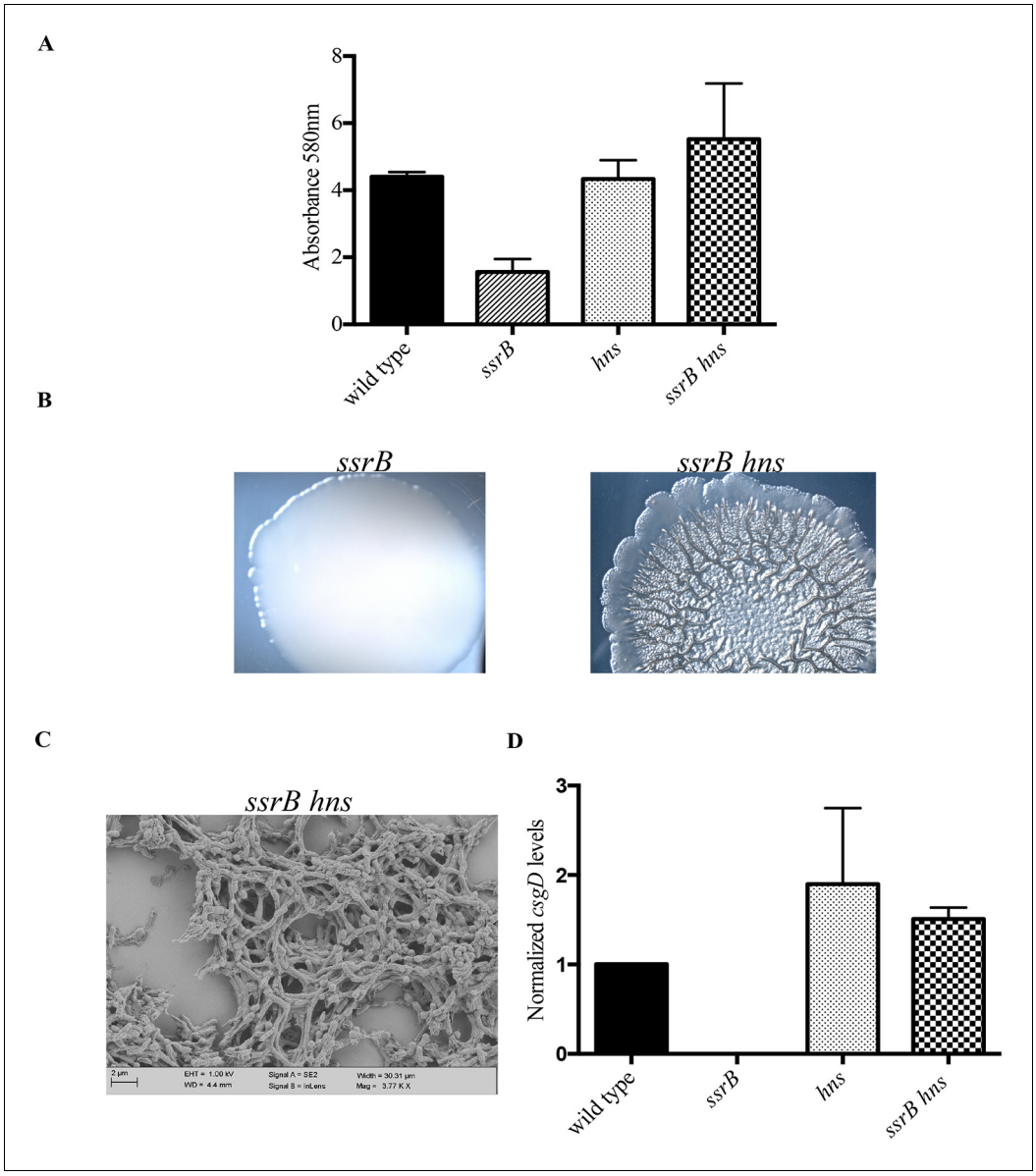

Figure 4. *hns* deletion rescues biofilm formation in the *ssrB* mutant as shown by Crystal violet staining. (**A**) The amount of biofilms formed is higher in the wild type, *hns* and *ssrB hns* strains compared to the *ssrB* null, n = 3, Mean ± SD, $p < 0.0001$. Source data file: ***Figure 4—source data 1***. Macrocolony phenotype (**B**) *ssrB hns* forms a highly rugose and dry macrocolony, while the *ssrB* macrocolony was smooth and mucoidy. SEM imaging (**C**) *ssrB hns* biofilms were covered by a thick extra-cellular matrix; scale bar = 2 µm. (**D**) qRT-PCR: *csgD* levels were restored in the *ssrB hns* strain and were higher than the wild type ($p < 0.03$) and the *ssrB* mutant ($p < 0.003$) against *rrsA* transcripts as a control. Note that the normalized *csgD* levels in the *ssrB* null were 0.0009, too low for the scale. n = 2, Mean ± SD. Source data file: Source data file: ***Figure 4—source data 2***.

DOI: http://dx.doi.org/10.7554/eLife.10747.017

The following source data is available for figure 4:

Source data 1. Source data for crystal violet staining in ***Figure 4A***.

DOI: http://dx.doi.org/10.7554/eLife.10747.018

Source data 2. Source data for Real-time qRT-PCR in ***Figure 4D***.

DOI: http://dx.doi.org/10.7554/eLife.10747.019

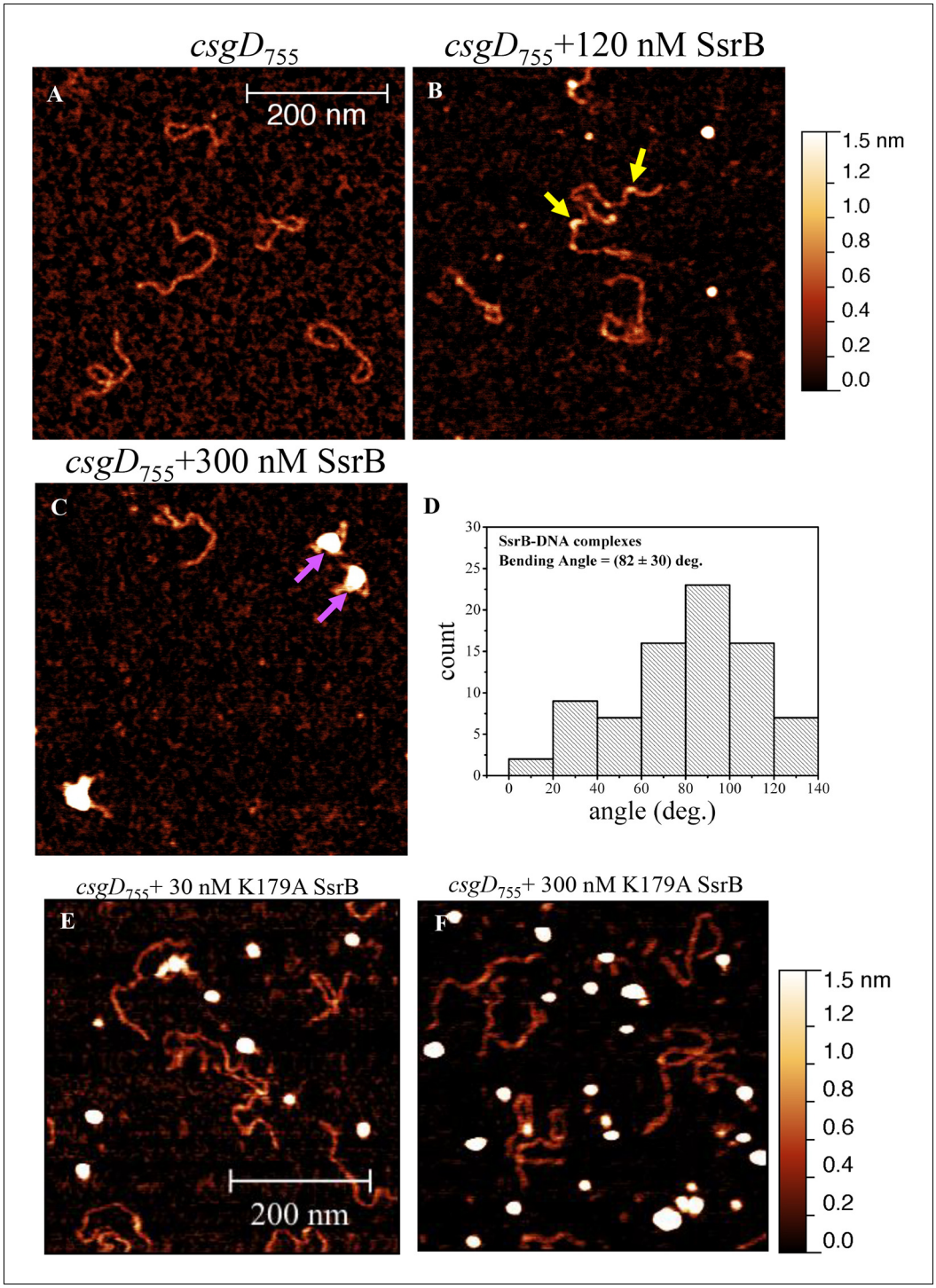

Figure 5. SsrB binds upstream of *csgD*. (**A**) AFM images of the 755 bp *csgD* regulatory region ($csgD_{755}$). (**B**) At 120 nM SsrB, distinct areas of SsrB binding were visualized as sharp bends (yellow arrows). (**C**) At 300 nM SsrB, areas of condensation (pink arrows) were observed. (**D**) Binding of SsrB bends the DNA by an average angle of 82° (for the naked DNA angle, refer to ***Figure 5—figure supplement 2*** and for analysis refer to Supplementary method), Scale bar = 200 nm as in (**A**). (**E**) and (**F**) The SsrB mutant, K179A SsrB, which is defective in DNA binding, was unable to bind $csgD_{755}$ both at 30 nM or 300 nM; Scale bar = 200 nm.

DOI: http://dx.doi.org/10.7554/eLife.10747.020

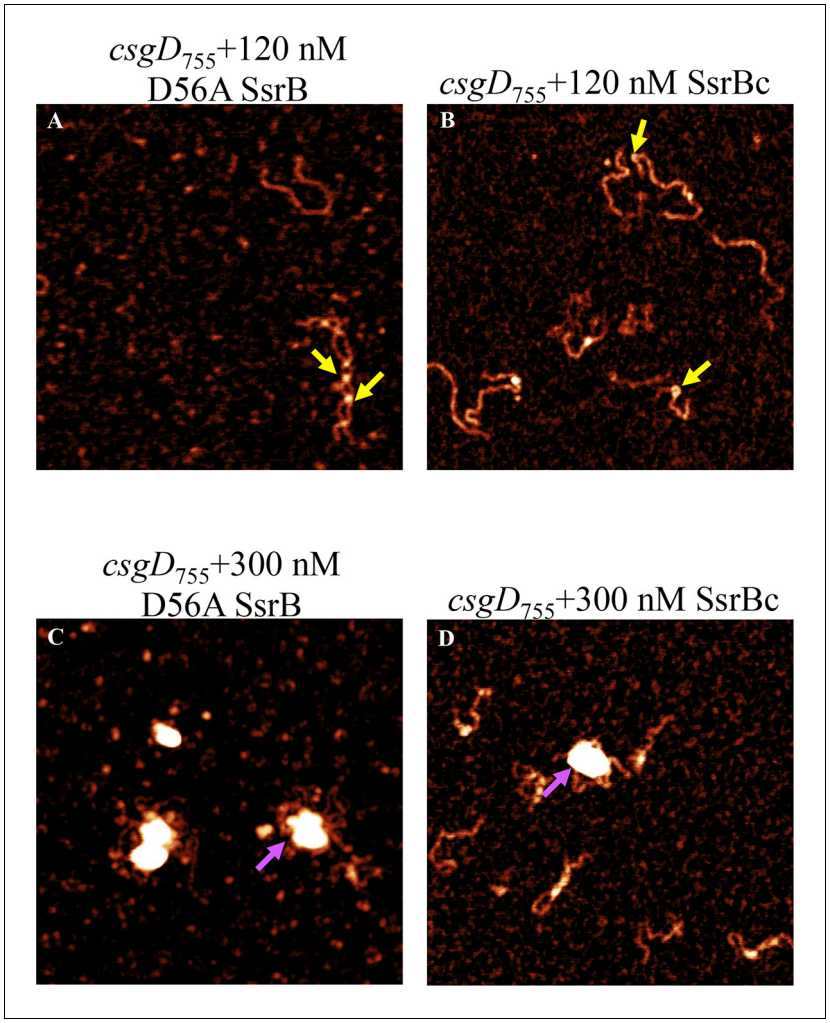

Figure 5—figure supplement 1. AFM images of the 755 bp *csgD* regulatory region ($csgD_{755}$) (**A**) with 120 nM D56ASsrB and (**B**) SsrBc. Distinct areas of binding were visualized as sharp bends (yellow arrows) and as areas of condensation (pink arrows) at 300 nM D56A SsrB (**C**) and SsrBc (**D**); Scale bar = 200 nm as in ***Figure 5A***.
DOI: http://dx.doi.org/10.7554/eLife.10747.021

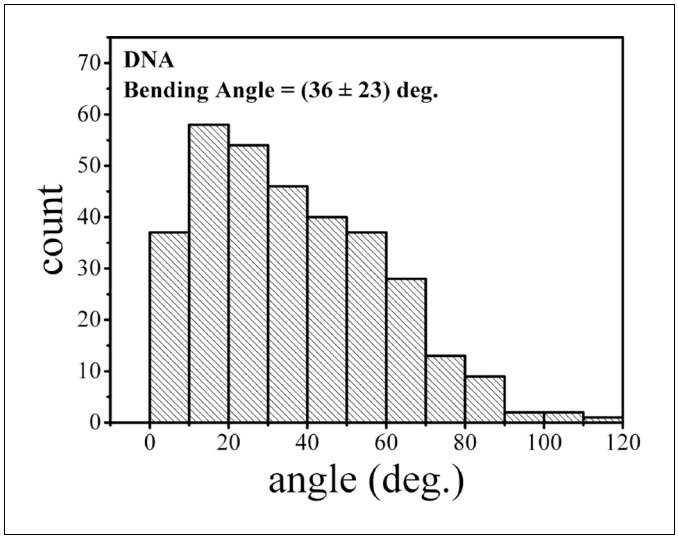

Figure 5—figure supplement 2. Bending angle of the naked *csgD*$_{755}$ fragment.
DOI: http://dx.doi.org/10.7554/eLife.10747.022

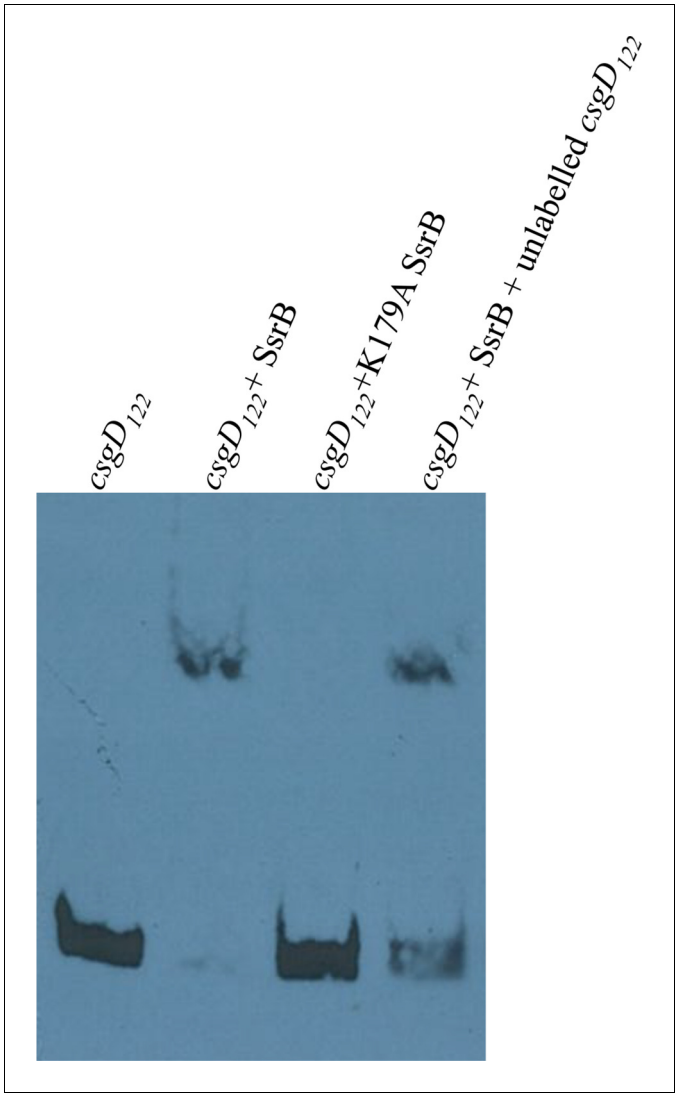

Figure 5—figure supplement 3. Electrophoretic mobility shift assay with the 122 bp *csgD* regulatory region, $csgD_{122}$, showing a DNA-protein complex in the presence of SsrB. The K179A SsrB mutant did not bind to $csgD_{122}$. Addition of competitor unlabelled $csgD_{122}$ fragment decreased the SsrB-DNA complex as apparent by an increase in free, labelled $csgD_{122}$.

DOI: http://dx.doi.org/10.7554/eLife.10747.023

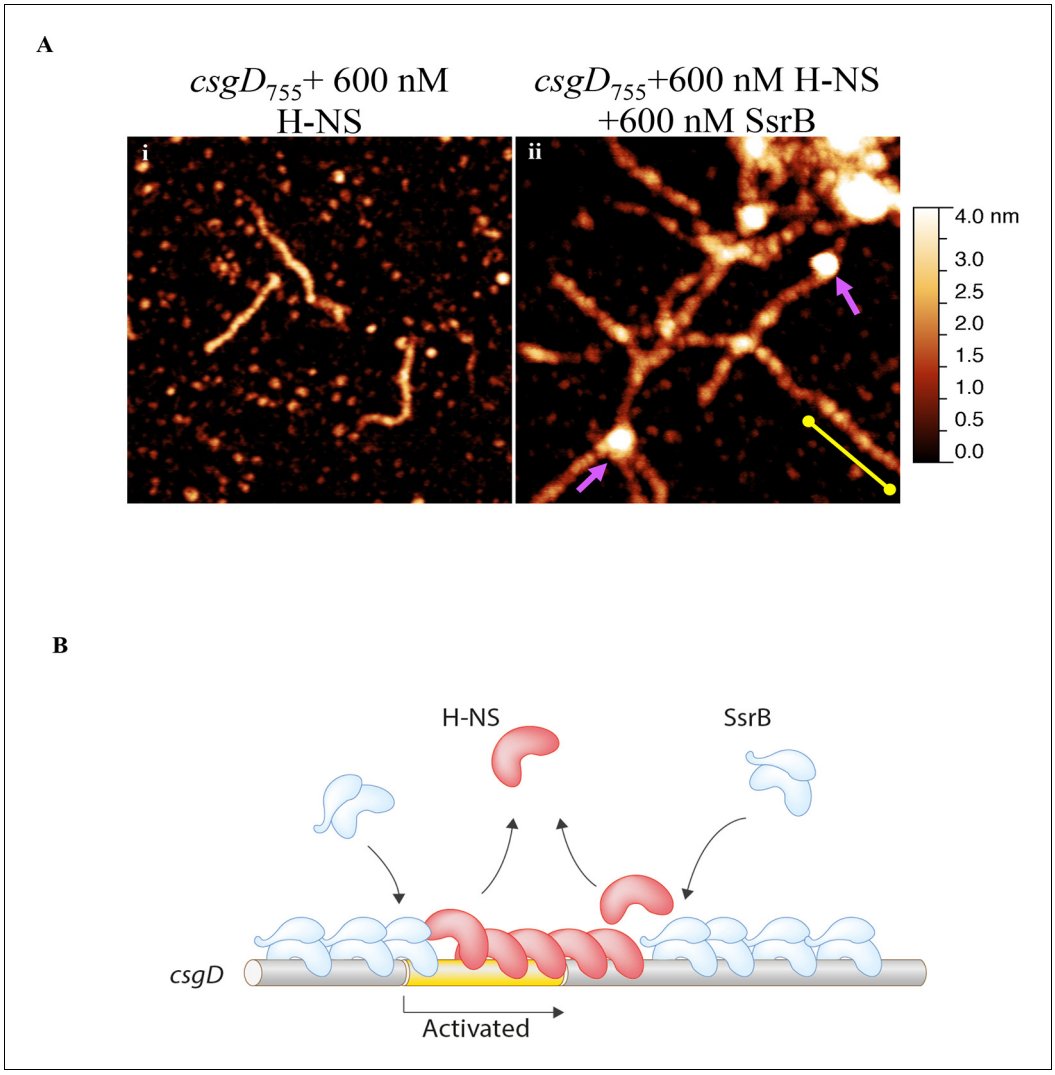

Figure 6. SsrB condenses H-NS bound *csgD* DNA. (**A**) (i) AFM imaging in the presence of 600 nM H-NS shows a straight and rigid filament on $csgD_{755}$. (ii) Addition of 600 nM SsrB to the H-NS bound *csgD* DNA resulted in areas of condensation (pink arrows; an 'SsrB signature') along with a few areas where the straight H-NS bound conformation persisted (yellow line; an 'H-NS signature'); Scale bar = 200 nm as in ***Figure 5A***. (**B**) A model for the mechanism of anti-silencing by SsrB at *csgD* wherein SsrB likely displaces H-NS from the ends of a stiffened nucleoprotein filament and relieves the blockade on the promoter for RNA polymerase to activate transcription. For details refer to (***Winardhi et al., 2015***).

DOI: http://dx.doi.org/10.7554/eLife.10747.024

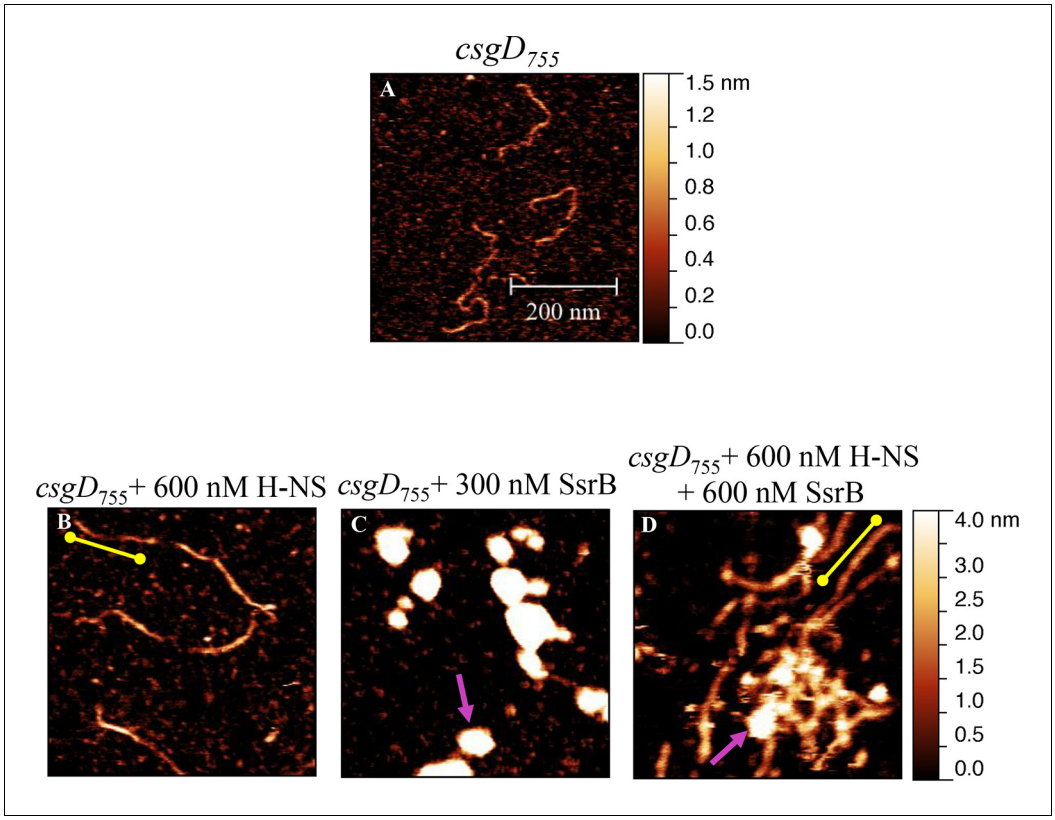

Figure 6—figure supplement 1. Liquid AFM imaging of (**A**) the 755 bp *csgD* regulatory region. (**B**) In the presence of 600 nM H-NS, a straight and rigid filament was observed (yellow line). (**C**) In the presence of 300 nM SsrB, areas of condensation were evident (pink arrow). (**D**) Addition of 600 nM SsrB to the H-NS bound *csgD* DNA resulted in areas of condensation (pink arrows; an 'SsrB signature') along with a few areas where the straight H-NS bound conformation persisted (yellow line; an 'H-NS signature'); Scale bar = 200 nm.

DOI: http://dx.doi.org/10.7554/eLife.10747.025

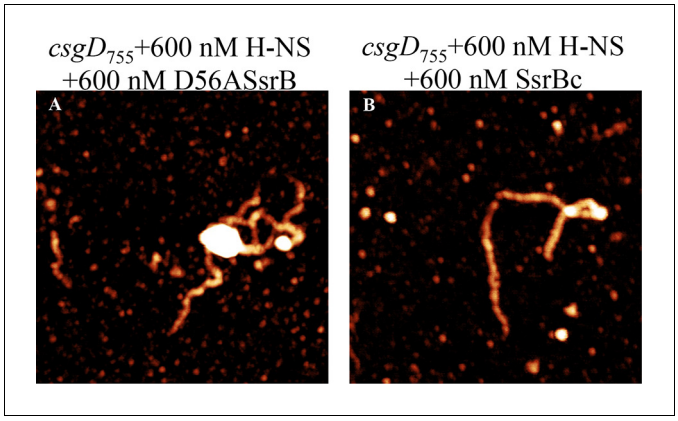

Figure 6—figure supplement 2. SsrB D56A and SsrBc condense H-NS-bound *csgD* DNA. AFM imaging in the presence of H-NS shows areas of condensation upon addition of (**A**) 600 nM D56ASsrB and (**B**) 600 nM SsrBc; Scale bar = 200 nm as in ***Figure 5A***.

DOI: http://dx.doi.org/10.7554/eLife.10747.026

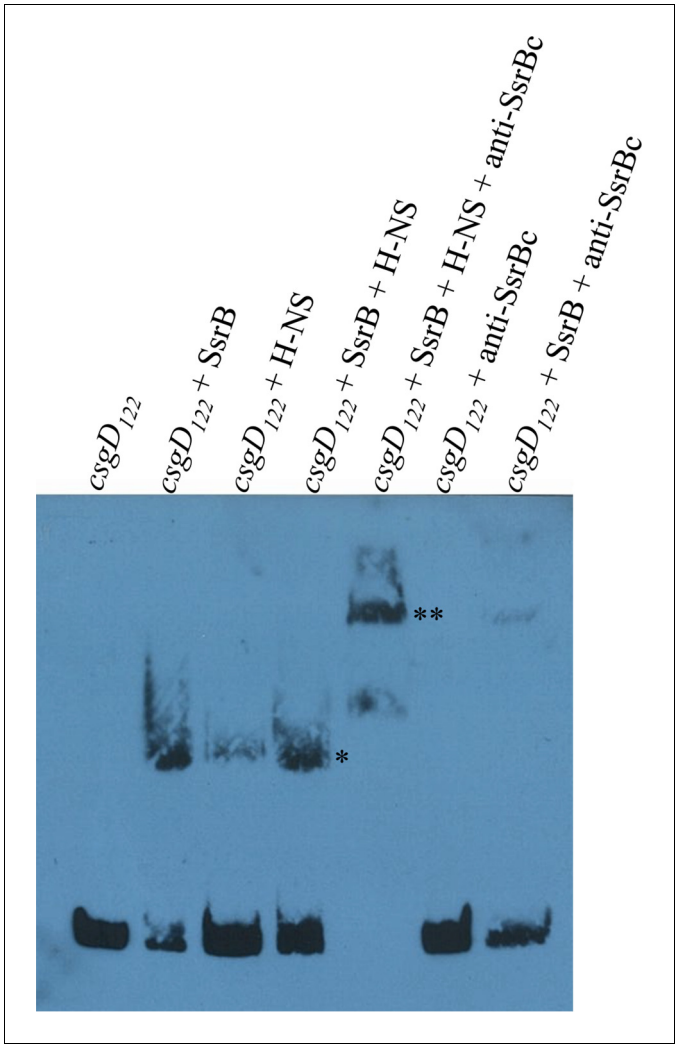

Figure 6—figure supplement 3. SsrB and H-NS form a complex on *csgD*. Electrophoretic mobility shift assay with the 122 bp *csgD* regulatory region, $csgD_{122}$ (left to right); in the presence of SsrB and H-NS, the DNA-protein complex (*) is super-shifted in the presence of anti-SsrBc serum (**). A DNA-protein complex is also observed when SsrB and H-NS were present alone. Note the absence of any complex in a control reaction with $csgD_{122}$ and anti-SsrBc, while anti-SsrBc recognizes the SsrB-$csgD_{122}$ complex.

DOI: http://dx.doi.org/10.7554/eLife.10747.027

tgctgtcaccctggacctggtcgtacatagcgaaaattatctattaccttgttagcgacatgcgtttttttgttaacgcgtcgttacgatgaagagtat
gtccgtggaaacatttttaataactcacccacgcgtggtattttgttatttaagctcataccaaagtgctaataaaacgatagccatgtgatttttta
taattgatttttggccacagaagatagtgtatcgcgcacctaaaaaatgaagtgttggtgtgtgttatgccgccatggggatgttcttatgcttccc
atgtggggcaatacgcacaagacgtgacacacttcgtttttttttgtctttgtgctgtccaggttaatgccacgtctcaaatttttaagaaaaaataaa
atcaaaacataacatataataattaaaatgattaaaaatcaatgaattattataatttgtatgatttttttaaatctatgcaataacagcgaaatgt
ac^{-122}aactttactatcaaatctaaacttcaaaaaaacccaaaaacaacattttaatatatatttttacatttggttacaagtttaacacttgctttaag
atttgtaatggctagattgaaaacagttaaaagtattttcgtaaatatttttctctttctggataatgggctatttcaacccacagcagtgcaacatc
tgtcagtacttctgg

Sequence in red: H-NS binding region (Gerstel et al., 2003)
Sequence in green boxes: SsrB binding motif (Feng et al., 2004)

Figure 6—figure supplement 4. The sequence of the 755 bp *csgD* regulatory region indicating the H-NS binding region according to ***Gerstel et al. (2003)***; and the SsrB binding motif as found by ***Feng et al. (2004)***.
DOI: http://dx.doi.org/10.7554/eLife.10747.028

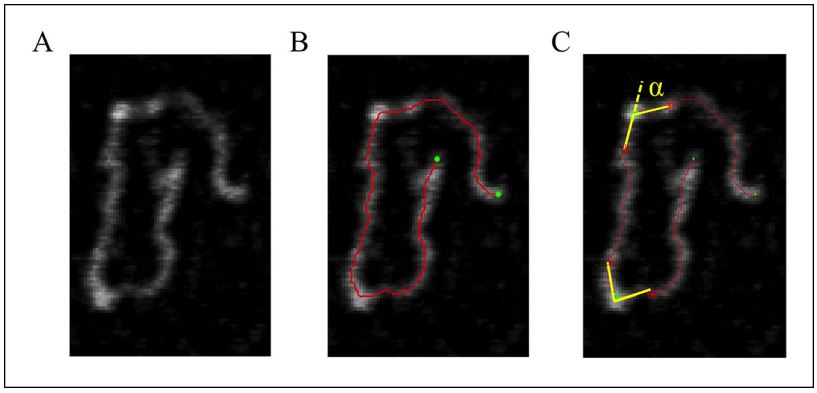

Figure 7. DNA tracing and bending angle measurement. (**A**) The original AFM image as processed with the Gwyddion software. (**B**) A Matlab code was used to trace the DNA in the AFM images. The digitized binary line represents the DNA backbone (red line), with the two end points marked by green dots. (**C**) For the bending angle measurement, a point along the red line was manually selected as the binding location of SsrB on DNA (green asterisk). The red asterisks indicate two points that are 15 nm upstream and downstream from this protein-binding site. Linear interpolation of points scattered along the green and red asterisk was used to plot a straight line between these points (yellow line). The angle between the yellow lines (α) is determined as the bending angle of SsrB; 81 such measurements were made. The same procedure was followed for the control AFM images of $csgD_{755}$, 327 such measurements were made.

DOI: http://dx.doi.org/10.7554/eLife.10747.031